The feasibility of thermal imaging as a future portal imaging device for therapeutic ultrasound

Piero Miloro[a*], John Civale[b], Ian Rivens[b], Adam Shaw[a]

[a] Acoustics and Ionizing Radiation Division, National Physical Laboratory, Hampton Road, Teddington, TW11 0LW, UK

[b] Therapeutic Ultrasound, Division of Radiotherapy and Imaging, Joint Department of Physics, Institute of Cancer Research : Royal Marsden NHSF Trust, Sutton, Surrey, SM2 5NG UK

* Correspondence to: Piero Miloro, AIR Division, National Physical Laboratory, Hampton Road, Teddington, TW11 0LW, UK. Tel +44 (0)20 8943 7188. E-mail: piero.miloro@npl.co.uk

Abstract

This technical note describes a prototype thermally-based portal imaging device which allows mapping of the energy deposition on the surface of a tissue mimicking material in a Focused Ultrasound Surgery (FUS) beam by using an infrared camera to measure the temperature change on that surface. The aim of the work is to explore the feasibility of designing and building a system suitable for rapid Quality Assurance (QA) use with both ultrasound and magnetic resonance (MR) imaging guided clinical therapy ultrasound systems. The prototype was tested using an MR guided Sonalleve FUS system (with the treatment couch outside the magnet bore). The system's effective thermal noise was 0.02 ºC, and temperature changes as low as 0.1 ºC were easily quantifiable. The advantages and drawbacks of thermal imaging for QA are presented through analysis of the results of an experimental session.

Keywords: High Intensity Focused Ultrasound dosimetry, Quality Assurance, Thermal mapping, Acoustic field evaluation, Magnetic Resonance guided Focused Ultrasound Surgery, Infrared camera

Introduction

The increasing number of devices and applications of Focused Ultrasound Surgery (FUS), also known as High Intensity Focused Ultrasound (HIFU), poses a significant challenge in terms of standardization of measuring and reporting ultrasound dosimetry, and there is a growing need for fast, reliable and accurate Quality Assurance (QA) strategies (Civale et al. 2015). HIFU transducers are often inextricably embedded in the clinical device and most conventional strategies for pressure mapping and power measurement of acoustic fields are difficult to apply in routine clinical practice (ter Haar et al. 2015). The use of multi-element transducer arrays generates a vast range of configurations that could need to be tested.

In radiotherapy, photographic film has been used to map the spatial distribution of energy incident on a specific plane since the 1950s (Granke et al. 1954). More recently, EPIDs (electronic portal imaging devices) have been developed (Heijmen et al. 1995) which record the energy distribution digitally (for instance using amorphous silicon detector) instead of on films. EPIDs offer advantages both as relative mapping and as dosimetric measurement devices (van Elmpt et al. 2008).

The use of thermal imaging acquired by infrared (IR) cameras has recently been proposed as a potential strategy for fast quantitative measurement of both diagnostic (Yamazaki, 2008) and high power acoustic fields (Shaw and Nunn 2010). Advantages of thermal imaging are the speed of 2D data acquisition, good spatial resolution and wide dynamic range. However, infrared radiation (wavelength ~10 μm) is strongly absorbed by water, so an air path is required between the camera and target, which results in a highly ultrasonically reflective interface at the plane of measurement. Recent advances include recording the temperature of the interface between air and Tissue Mimicking Materials (TMMs) (Myers and Giridhar 2011) or strongly absorbing thin layers (Shaw et al. 2011). Khokhlova et al. (2013) have shown that the temperature distribution near the reflecting air interface closely follows the distribution of the temporal-average intensity in the incident beam.

The aims of this study were to test whether the IR camera can be used close to a Magnetic Resonance (MR) imaging scanner without significant thermal image artefacts and map the in-plane temperature distributions in the same configuration used for therapy. Future work will compare the

results with other measurement systems such as hydrophone mapping and acoustic holography (Kreider et al., 2013).

In this work, the device has been tested on a Philips Sonalleve MR guided FUS system installed at ICR/Royal Marsden Hospital (Sutton, UK).

Materials and methods

Hardware

A compact (46 x 56 x 90 mm), USB-powered PI-200 IR camera (Optris Infrared Thermometers, Germany) with 120 x 160 pixel resolution and a maximum frame rate of 128 Hz was used. The claimed noise-equivalent temperature is 80 mK, and temperature data can be displayed and exported by the camera software with a resolution of 0.1 ºC. However, by processing directly raw data files it has been possible to improve the resolution to 0.02 ºC. The camera is mounted within a 3D-printed waterproof holder (Figure 1) composed of two flanges sealed with O-rings. A 100 mm diameter, 6 μm thick Mylar membrane was the measurement surface. The camera was fixed to the base and its distance from the membrane can be varied between approximately 30 and 130 mm, in order to provide spatial resolution between 0.07 mm to 0.3 mm per pixel and a field of view of 12 x 9 mm to 52 x39 mm, respectively. A 10 m USB cable with built-in amplification chipset (BlueRigger Active Extension, USA) was connected to the IR camera passed through the holder base via a waterproof seal.

For the configuration shown in Figure 1, a 65 mm high cylinder of TMM was used as the absorbing target, pushed against the front membrane using an additional flange. The target size allowed measurement of both the pre- and post-focal fields of the Philips Sonalleve system. The TMM is an agar-based gel whose formulation is given in IEC60601-2-37 (IEC 2008). The main acoustic properties of the TMM are: an amplitude attenuation coefficient which is almost linear with frequency (0.49 ± 0.05 dB cm^{-1} MHz^{-1}), a speed of sound of 1540 m s^{-1} ± 1%, density of 1070 ± 30 kg m^{-3} and specific heat capacity of 3770 J kg^{-1} K^{-1} ± 3% (Brewin et al. 2008).

The tests were performed using a Philips Sonalleve MR guided FUS system at a distance of approximately 1 m from the edge of the magnet bore of a 3.0 T Philips Achieva MR imaging scanner (i.e. the Sonalleve patient bed was in its 'pulled-out' position). The 256 element array transducer, with a 140 mm geometric focal length and 140 mm diameter can be operated at 1.2 or 1.45 MHz. It is mounted within the patient bed in an oil-filled chamber on a 5 degree of freedom positioning system.

Experimental procedure and data processing

The assembly was acoustically coupled to the Sonalleve transducer using degassed water between the coupling membrane of the HIFU system and the TMM. The axial distance between the transducer and the coupling membrane of the HIFU system was varied over a range of 50 mm around the transducer's homing position. Sixteen measurements were carried out at different axial positions and input powers (see Table 1). For each experiment, the transducer was driven in continuous mode at 1.2 MHz for 3 s. Thermal data acquisition was initiated 10 s before the start and stopped 27 s after the end of the insonation Thermal image sequences were saved at a frame rate of 20 Hz, about 20 times the rate for MR thermometry. The automatic flag (i.e. self-recalibration of the IR camera) was disabled during the acquisitions.

Data was processed in a custom made MatLab programme. The following algorithm was applied: *i.* Frames earlier than 5 s before the start of insonation were ignored. *ii.* 100 frames obtained immediately before exposure were averaged to provide a baseline image for suppression of artefacts, including removing the reflection of the camera. *iii.* Changes in the average pixel value in a control region outside the beam were monitored to correct for common-mode drift of the thermal sensors. *iv.* A triangular-weighted temporal-smoothing function was applied (typically over ±3 frames). *v.* A MatLab built-in 2D adaptive low-pass filter for intensity images was applied (typically over a 3 x 3 pixel square) (Lim 1990). *vi.* The corrected and smoothed pixel values were transformed into temperature values through the calibration table provided by the camera manufacturer. *vii.* Baseline and common drift were subtracted from each frame, to obtain a temperature change map. The number of frames and pixels over which the filters were applied could be adjusted if necessary to achieve the best compromise between noise levels and spatial or temporal resolution. An example of a processed

file is shown in Figure 2. Differences between processed and raw data can be significant due to the cumulative effect of both the common-mode drift and residual cooling from previous experiments (step iii of the processing algorithm).

The x/y position and the value of the highest temperature pixel for each exposure were obtained, as were the position and value of the maximum rate of change of temperature rise calculated in the linear region of the $T(t)$ curve, i.e. within the first second of insonation, in order to reduce the effects of heat diffusion. The start of insonation was also automatically detected using the same *T(t)* curve. The *in situ* spatial peak temporal averaged intensity (I_{spta}) was estimated from the maximum rate of change of temperature, assuming negligible thermal conductivity, using:

$$I_{spta} = \frac{\rho C \frac{\partial T}{\partial t}}{2\alpha} \quad (1)$$

where α is the amplitude attenuation coefficient (expressed in Np m^{-1} at the centre frequency), ρ is the density and C is the specific heat capacity. Finally, the width of the beam was calculated as the maximum distance between two points with local intensity value greater than -6 dB of I_{spta} in the plane (if not otherwise specified).

Results

MR Compatibility

The effect of the scanner's magnetic field on the IR camera was investigated by placing an optically opaque rubber sheet 3 mm thick over the front window of the system to give a constant and flat temperature distribution. The system was taken slowly towards the magnet whilst monitoring the temperature distribution continuously on a laptop. Any thermal drift or distortion at a distance of approximately 1 m from the bore was less than 0.1^{o}C and not visible. Also, none of the components of the assembly was subject to obvious magnetic attraction. At approximately 70 cm from the bore, USB communication was lost: it was not clear if this loss was due to a poor connection or caused by the magnetic field. However, it was decided to go no closer than 1 m for the later tests.

Experimental session

Results for the 16 exposures are reported in Figure 3 and summarized in Table 1. Data presented in this work represent the temperature at a depth of 65 mm in the TMM, so the acoustic wave is attenuated by approximately 7 dB (at the working frequency) before reaching the measurement surface. Measured rates of change of temperature raise ranged from 0.1 °C s^{-1} for Test 11 (position = 30 mm, power = 20 W) to 34 °C s^{-1} for Test 5 (position = 10 mm, power = 40 W), which correspond to estimated *in situ* I_{spta} values of 3.1 W cm^{-2} and 1026 W cm^{-2} respectively. Figure 3 indicates that the focus (narrowest beam and greatest intensity) coincided with the transducer's vertical position being about + 10 mm: moving to positions > 10 mm, meant that the measurement surface sensed the post-focal field. There was good repeatability of intensity measurements made in the same position (see e.g. the four tests at axial position = 0 mm in Figure 3 and Table 1). Furthermore, 40 W exposures showed approximately twice the temperature rise of those at 20 W, see e.g. Test 11 and 12 in Table 1, and Test 1 or 2 with Test 16, suggesting a 1:1 linear relationship between selected power and the temperature rise.

Figure 4 shows an example of the evolution with time after the end of insonation of a temperature profile close to the focal plane. The curves show the temperature over an axis perpendicular to the beam axis at 0, 2, 4, 6, 8 and 10 s after the end of exposure. The profiles are shown normalized with the peak temperature at each different time.

Figure 5 shows that the system allows to obtain spatial quantities from the analysis of the temperature distribution at the end of insonation in the plane transverse to the beam axis. The -6 dB area (relative to the maximum value in the image) is automatically detected by the post-processing code. Axial positions of 15, 20 and 30 mm are shown (Tests 6, 13 and 12 respectively in Table 1) and the temperature distribution gives a quantitative measure of the magnitude of the side lobes. For the tests with the transducer positioned at +15 mm (measurement surface 5 mm beyond the focus), the -6 dB beamwidth was ~5 mm and there was a single main lobe. For the other two positions, ring structures consistent with the appearance of side lobes were detected. In these cases the position of maximum temperature rise was 3 mm and 6 mm away from the position of maximum temperature in

the focal plane (for the tests at +20 mm and +30 mm, respectively). It is interesting to observe that the position of the visible hot spots in the ring structure in Figure 5 (Right) suggests an 8-fold symmetry.

Data acquisition and processing when the measurement surface is close to the focal plane, in the specific test session when I_{spta} exceeded 250 W cm^{-2}, presented several difficulties. Figure 6 shows the temperature change map and the peak temperature evolution for the point of highest temperature in one test in the focal plane. Two effects can be seen, the loss of beam symmetry and the departure from the expected temperature-time profiles.

Discussion

Infrared imaging has been shown to be capable of rapid 2D measurement of temperature changes in a well characterized TMM before, during and after the application of focused ultrasound via a MR guided FUS system. The device cannot be assumed to be MR compatible, because no attempt was made to image with it in place. Furthermore, it should be well suited for use with US guided HIFU systems.

The main strength of the IR camera strategy is that information for a whole cross sectional plane of an ultrasound beam can be acquired in seconds with good spatial (0.3 mm was demonstrated), thermal (0.1 C s^{-1}) and temporal resolution (up to 128 Hz) and a wide dynamic range. Even if typical measurement time was 40 seconds, this is still orders of magnitude faster than obtaining a hydrophone plot at 0.3 mm spatial resolution over a width that was large enough to include the first side lobe ring, e.g. at 30 mm pre- or post-focal peak. On this basis, the IR system could fulfil the same role for FUS as an EPID does for radiotherapy and the name uPID (ultrasonic portal imaging device) seems appropriate.

Some problems occurred when we tried to measure intensity higher than 250 W cm^{-2}. Figure 6 shows the 2D maps and temperature-time curve obtained at the focal plane. The figure shows features that look like artefacts during heating. These can be caused by the occurrence of cavitation (a similar profile has been observed by Maruvada et al. (2012) in swine muscle and TMM), by melting of the gel, or by the separation of the membrane from the TMM due to the radiation force exerted by

the HIFU beam. A future task will be to identify the cause and find an experimentally robust strategy for making measurements at high intensity.

Conclusions

This work has presented a prototype system which uses thermal imaging as a potential future ultrasonic portal imaging device (uPID) for clinical MR and US guided HIFU systems, following the model adopted in clinical radiotherapy.

The system can rapidly map the distribution of energy in a carefully specified plane at spatial resolution similar to that of hydrophone measured beam plots, by monitoring temperature with an IR camera. The system was able to detect temperature changes as low as 0.1 °C and intensity values from ~3 W cm^{-2} to ~1000 W cm^{-2} were estimated (using Eq. 1), at a frame rate of 20 Hz. To the authors' knowledge this is the first time that IR thermometry has been exploited to measure the output of an extra-corporeal clinical FUS transducer *in situ*, without dismounting the device from its operational position and/or clinical drive system.

Further developments are required in both theoretical and experimental design to improve the uncertainties involved in estimating absolute acoustic quantities such as I_{spta}. Theoretical modeling of the effect of the air interface on acoustic propagation and hence thermal energy deposition is needed, along with ways of improving experimental repeatability, especially when higher intensity fields (I_{spta} > 250 W cm^{-2}) are investigated. Nevertheless, these initial results suggest that the uPID approach is worth pursuing.

Acknowledgement

This work was supported in part by the European Metrology Research Programme (Project HLT-03: Dosimetry for Ultrasound Therapy) with funding by the European Union. The EMRP is jointly funded by the EMPR participating countries within EURAMET and the European Union). We are also grateful for funding and support from the Focused Ultrasound Foundation (FUSF Centre of Excellence) and Philips Healthcare, and the EPSRC.

References

Bobkova S., Gavrilov L., Khokhlova V., Shaw A., & Hand, J., Focusing of high-intensity ultrasound through the rib cage using a therapeutic random phased array. Ultrasound Med Biol 2010; 36(6): 888-906.

Brewin M. P., Pike L. C., Rowland D. E., & Birch, M. J., The acoustic properties, centered on 20 MHz, of an IEC agar-based tissue-mimicking material and its temperature, frequency and age dependence. Ultrasound Med Biol 2008; 34(8): 1292-1306.

Civale J., Rivens I., & ter Haar G. Quality assurance for clinical high intensity focused ultrasound fields. Int J Hyperthermia 2015; 31(2): 193-202.

Giridhar D., Robinson R. A., Liu Y., Sliwa J., Zderic V., & Myers M. R., Quantitative estimation of ultrasound beam intensities using infrared thermography—Experimental validation. J Acoust Soc Am 2012; 131(6): 4283-4291.

Granke R.C., Wright K. A., Evans W. W., Nelson J. E., & Trump J. G., The film method of tissue dose studies, Am J Roentgen 1954; 72:302

Heijmen B. J. M., Pasma K. L., Kroonwijk M., Althof V. G. M., De Boer J. C. J., Visser A. G., & Huizenga H., Portal dose measurement in radiotherapy using an electronic portal imaging device (EPID). Phys Med Biol 1995; 40(11): 1943.

International Electrotechnical Commission. Particular requirements for the basic safety and essential performance of magnetic resonance equipment for medical diagnosis. IEC 60601-2-37:2008

Khokhlova V. A., Shmeleva S. M., Gavrilov L. R., Martin E., Sadhoo, N. & Shaw, A., Infrared mapping of ultrasound fields generated by medical transducers: Feasibility of determining absolute intensity levels. J Acoust Soc Am 2013; 134(2): 1586-1597.

Kreider, W., Yuldashev, P. V., Sapozhnikov, O., Farr, N., Partanen, A., Bailey, M. R., & Khokhlova, V. A. Characterization of a multi-element clinical HIFU system using acoustic holography and nonlinear modeling. IEEE T Ultrason Ferr 2013, 60(8), 1683-1698.

Lim J. S., Two-Dimensional Signal and Image Processing, Englewood Cliffs, NJ, Prentice Hall, 1990, p. 548

Maruvada, S., Liu, Y., Pritchard, W. F., Herman, B. A., & Harris, G. R., Comparative study of temperature measurements in ex vivo swine muscle and a tissue-mimicking material during high intensity focused ultrasound exposures, Phys Med Biol 2012, 57(1), 1-19.Myers M. R., & Giridhar, D., Theoretical framework for quantitatively estimating ultrasound beam intensities using infrared thermography, J Acoust Soc Am 2011; 129(6): 4073-4083.

ter Haar G., Rivens I., Civale J., Bunton C., & Symonds-Tayler R., Quality assurance and field characterisation for MRgHIFU treatments: their need and the challenges presented. J Ther Ultrasound 2015; 3(Suppl 1): O66.

Shaw A., & Nunn J., The feasibility of an infrared system for real-time visualization and mapping of ultrasound fields. Phys Med Biol 2010; 55(11): N321.

Shaw A., Khokhlova V., Bobkova S., Gavrilov L., & Hand, J., Calibration of HIFU intensity fields measured using an infra-red camera. J of Physics: CS 2011; 279(1): 012019

van Elmpt W., McDermott L., Nijsten S., Wendling M., Lambin P., & Mijnheer B., A literature review of electronic portal imaging for radiotherapy dosimetry. Radiother Oncol 2008; 88(3): 289-309.

Yamazaki S., Investigation on the usefulness of the infrared image for measuring the temperature developed by transducer. IEEE Ultrasonics Symposium (IUS) 2008; p. 1698-1701.

Figures Captions

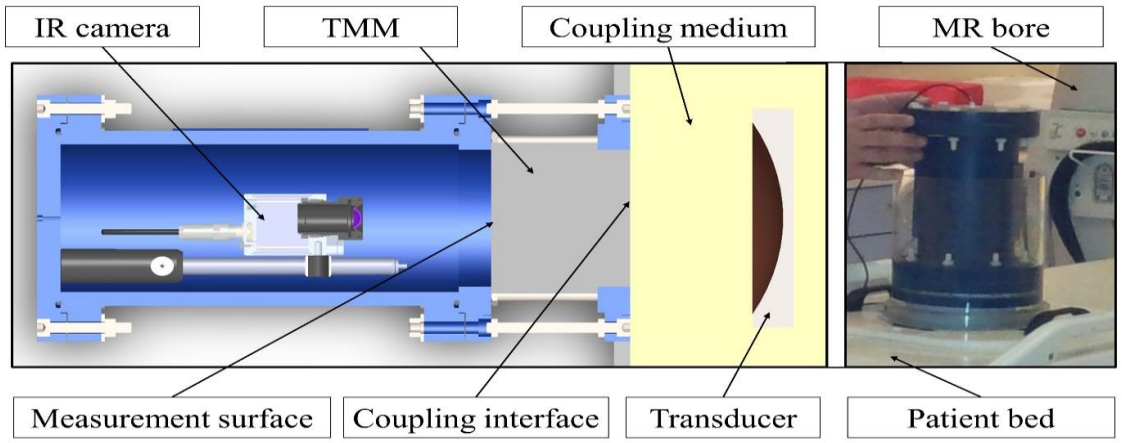

Figure 1. Experimental setup. Left: Sketch of a cross-section through the measurement device, Tissue Mimicking Material (TMM), coupling medium and ultrasound transducer. Right: The device positioned on the magnetic resonance bed of the Sonalleve system.

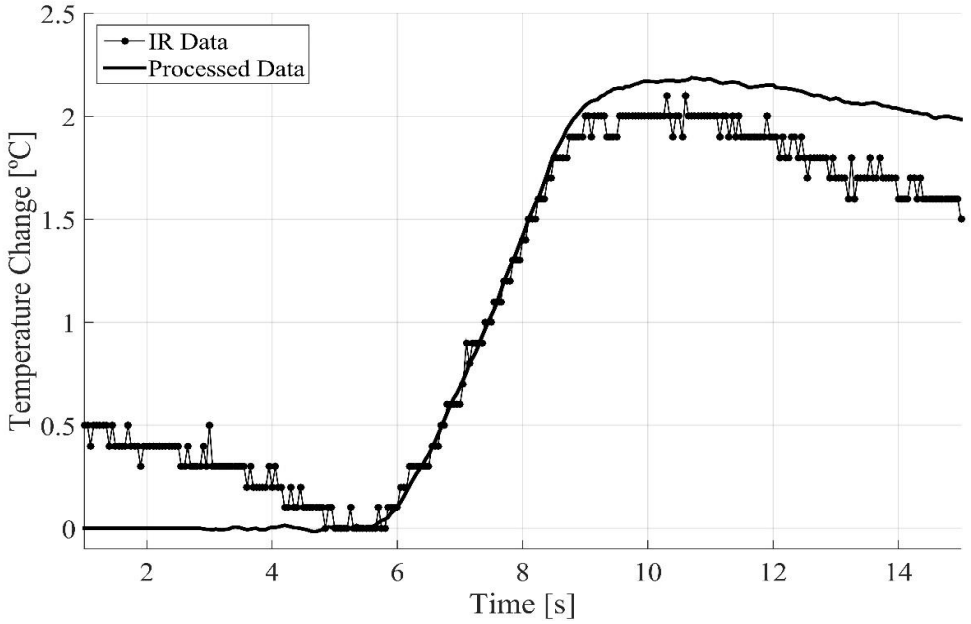

Figure 2. Results of the data processing algorithm. Infrared (IR) data is extracted from the imager software (resolution 0.1 °C), while processed data underwent the procedure described in the text.

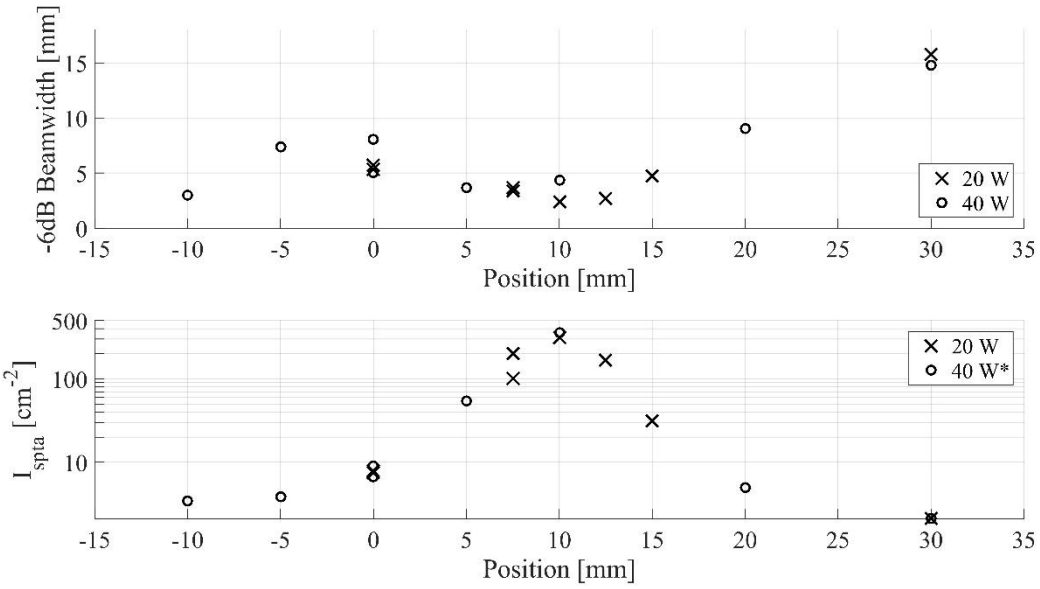

Figure 3. Results for the experimental session. Top: -6 dB beamwidth measured from thermal profiles. Bottom: spatial-peak temporal-averaged Intensity (I_{spta}) calculated from peak temperature gradient measurements at different axial positions relative to the transducer homing position; note that data for 40 W experiments has been divided by a factor 2 to compare directly with the 20 W results.

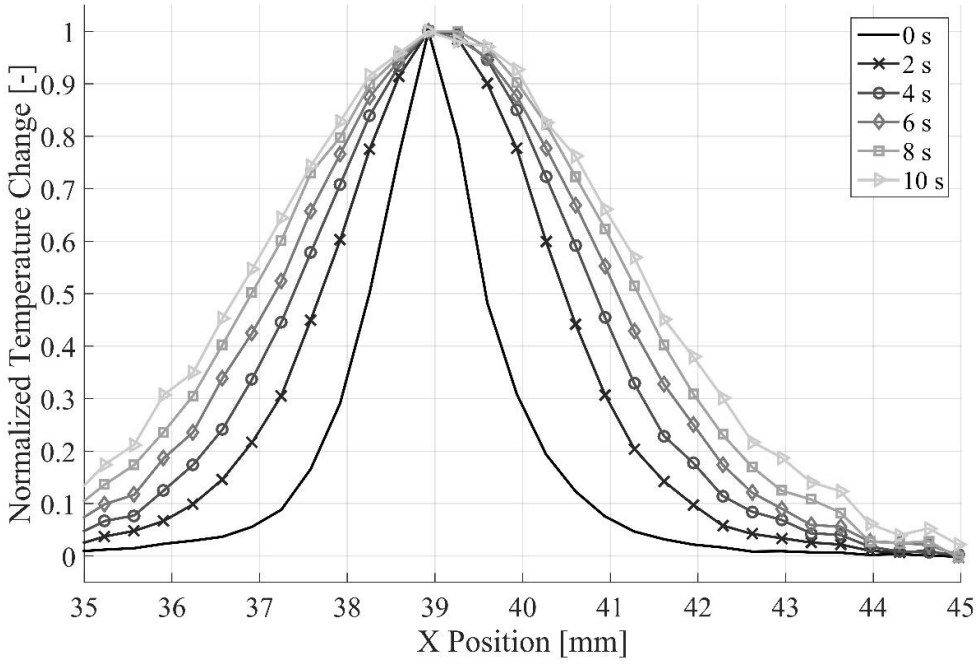

Figure 4. Temperature profile along a line perpendicular to the beam axis. Curves show values taken at different times after the end of insonation. The curve for each time is normalized to a peak temperature of 1 to emphasize the increasing width of the distribution.

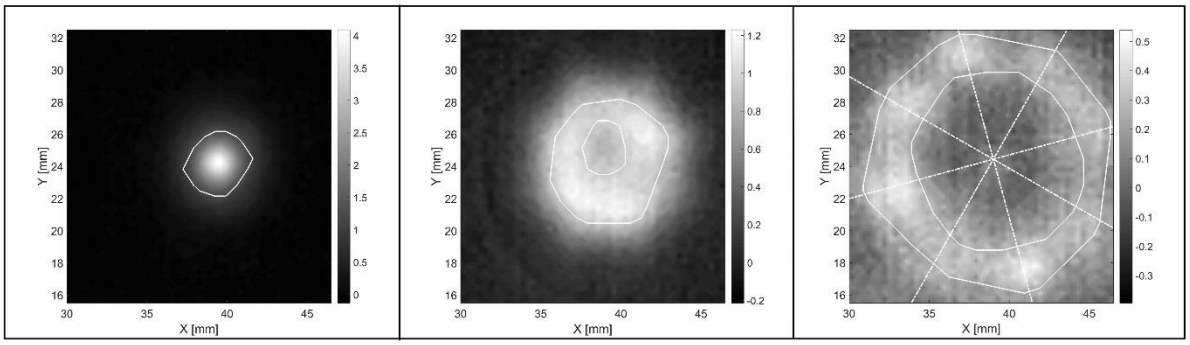

Figure 5. Temperature change maps obtained transverse to the HIFU beam. Axial positions are: 15 mm (Left), 20 mm (Centre) and 30 mm (Right), corresponding to measurement surface at 5 mm, 10 mm and 20 mm beyond the focal peak, respectively. At each position the -6 dB area (relative to the maximum within that plane) is outlined.

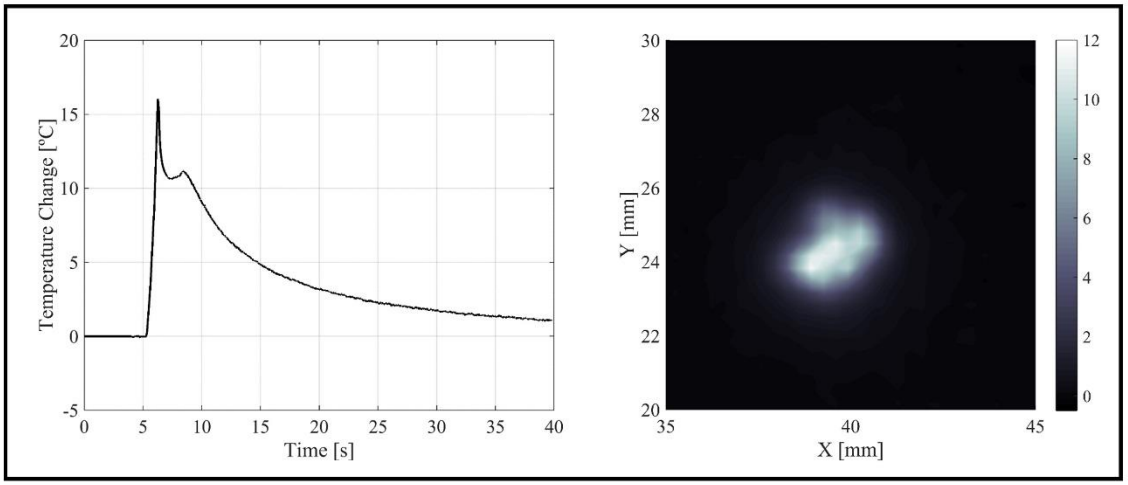

Figure 6. Temperature change curve and 2-D map for Test 8.

Tables

Table 1 Exposure parameters and results for the 16 experimental measurements. The position indicates the location of the Sonalleve transducer relative to its homing position. T_{max} indicates the peak temperature. The transducer was driven at 1.2 MHz for 3 s in each case.

Test ID	1	2	3	4	5	6	7	8	9	10	11	12	13	14	15	16
Position [mm]	0	0	0	5	10	15	12.5	10	7.5	7.5	30	30	20	-10	-5	0
Power [W]	20	20	40	40	40	20	20	20	20	20	20	40	40	40	40	40
T_{max} [°C]	1.1	1.1	2.7	11.3	18.1	4.1	12.4	15.7	9.3	15.8	0.3	0.6	1.2	0.8	1.1	2.2
dT/dt *[°C s^{-1}]*	0.4	0.4	0.9	4.3	34	1.6	8.4	16	4.9	11	0.1	0.2	0.4	0.3	0.4	0.6
I_{spta} [W cm^{-2}]	10.9	10.6	25.4	129	1026	45.8	252	487	146	323	3.1	5.6	11.9	10	11.1	19.1
Beamwidth [mm]	6.4	5.4	5.0	3.0	4.4	5.0	2.7	3.7	3.7	2.7	14	16	11	9.1	9.7	8.4